Journal of Catalysis **190,** 396–405 (2000)
doi:10.1006/jcat.1999.2755, available online at http://www.idealibrary.com on IDEAL®

Direct Conversion of *n*-Butane to Isobutene over Pt–MCM22

G. D. Pirngruber, K. Seshan, and J. A. Lercher[1]

Faculty of Chemical Technology, University of Twente, P.O. Box 217, 7500 AE Enschede, The Netherlands

Received August 4, 1999; revised November 2, 1999; accepted November 2, 1999

MCM22 is a very active and selective catalyst for the skeletal isomerization of butene. At temperatures up to 775 K, Pt–MCM22 gives good results in the dehydroisomerization of *n*-butane, achieving higher yields of isobutene than does Pt–ZSM5. Most notably, the formation of cracking products is low. Alternatively, MCM22 can also be used as an isomerization catalyst in combination with Pt–ZSM5 in order to increase the yield of isobutene in dehydroisomerization. A disadvantage of the MCM22 materials, however, is their moderate stability, especially at higher temperatures. During calcination/reduction of Pt–MCM22 partial dealumination of the framework occurs, leading to enhanced deactivation by coking.

Key Words: **dehydroisomerization of *n*-butane; MCM22; skeletal isomerization of *n*-butene.**

INTRODUCTION

The dehydroisomerization of *n*-butane to isobutene is a challenging reaction. Due to thermodynamic constraints of dehydrogenation it has to be carried out at high temperatures (above 750 K). Bifunctional catalysts for dehydroisomerization have to be optimized with respect to their dehydrogenation and isomerization activity, as well as their stability toward deactivation. It has been shown that Pt–ZSM5 is a good catalyst for the dehydroisomerization of *n*-butane (1). Its major shortcoming is the rather high selectivity to by-products at high conversions stemming from oligomerization/cracking of butenes on the acid sites. Better results should be achieved by using other Pt supports that have a higher selectivity to butene isomerization vs oligomerization/cracking than ZSM5. FER and TON are known as selective catalysts for butene isomerization (2–4). When Pt–FER and Pt–TON were tested for dehydroisomerization of *n*-butane, however, it turned out that besides the high selectivity of the parent zeolite in butene isomerization also other factors play a role (5). The zeolite support must also have a low activity for protolytic cracking of *n*-butane, which is a potential side reaction. Moreover, the manner in which Pt is dispersed and stabilized on the support is very important. High dispersion in the pores of the zeolite, such as found with Pt–FER, seemed to lead to a very *low* dehydrogenation activity (5).

MCM22 is a microporous material with a layered structure (6). Within the layers a two-dimensional sinusoidal channel system exists, which is accessible through 10-membered-ring apertures. Between the layers supercages are formed, defined by 12-membered rings. The cages are accessible through 10-membered-ring apertures. The two channel systems are not connected. The product pattern of MCM22 in the isomerization and hydrocracking of decane, a test reaction for the determination of unknown pore structures (7, 8), was similar to the product patterns of 10-membered-ring zeolites (9). Such zeolites have the right shape-selective properties for butene isomerzation (10, 11). Indeed, the successful application of MCM22 for this reaction was reported by Asensi *et al.* (12). Being suited for butene isomerization, MCM22 was also an interesting material for application in the dehydroisomerization of *n*-butane.

Since our earlier studies had shown that the SiO_2/Al_2O_3 ratio has a large influence on the catalytic performance (1, 5), we tested two MCM22 samples (with SiO_2/Al_2O_3 ratios of 25 and 35, respectively) for the dehydroisomerization of *n*-butane. In principle, even higher SiO_2/Al_2O_3 ratios should be beneficial (1, 5). The synthesis of highly siliceous MCM22 is difficult, however, and often leads to the formation of other crystal phases (13). In order to achieve a rather high ratio of metal to acid sites, which was identified to be beneficial for the catalyst performance (1, 5), we chose rather high metal loadings of 0.5–1 wt% Pt. The objective of the study was to evaluate the catalytic performance of Pt–MCM22 and correlate it with the physico-chemical properties of the materials.

EXPERIMENTAL

Catalyst Preparation

MCM22 with $SiO_2/Al_2O_3 = 35$ was received from Prof. J. Weitkamp, University of Stuttgart (ST). It had been prepared according to the procedure outlined in Ref. (14). In order to remove the template the sample was calcined in a flow of 70% N_2 and 30% air at 813 K for 15 h (ramp rate 2 K/min).

[1] Present address: Institute for Chemical Technology, Technische Universität München, Lichtenbergstr. 4, D-85748 Garching, Germany.

0021-9517/00 $35.00

MCM22 with $SiO_2/Al_2O_3 = 24$ was received from Shell Research and Technology Center Amsterdam (SR). It was prepared following the method of US patent 5.085.762 (15). After synthesis the sample was dried at 393 K and calcined at 813 K for 10 h (ramp rate 1.67 K/min).

Both samples were ion-exchanged with an aqueous solution of NH_4NO_3 in order to obtain the ammonium form. Pt was incorporated by ion-exchange with a dilute aqueous solution of $Pt(NH_3)_4(OH)_2$ (0.1 mg of Pt/l) and NH_3 (~2%), according to the method described in Ref. (1). After ion-exchange the samples were dried, calcined in air at 723 K for 2 h (ramp rate 0.5 K/min), and reduced in H_2 at 773 K for 2 h (temperature increment 5 K/min). The Pt loading was varied between 0.5 and 1 wt%.

Characterization

The elemental composition of the samples was determined by X-ray fluorescence (XRF). The crystal phase was determined by powder X-ray diffraction, using a Phillips PW3710 instrument in continuous scan mode. In order to quantify the crystallinity of the MCM22 samples, they were mixed in a 1 : 1 (m/m) ratio with α-Al_2O_3. The relative intensity of the reflections at $2\Theta = 10.1^\circ$ (102) and $2\Theta = 26.1^\circ$ (302), of MCM22, and at $2\Theta = 35.25^\circ$ (104), of α-Al_2O_3, was used for comparison of the samples.

For determining the Brønsted and Lewis acidities of the materials, the IR spectra of adsorbed pyridine were used. For this, the samples were pressed into self-supporting wafers (2–3 mg) and placed into a cylindrical oven, which in turn was attached to an IR cell with CaF_2 windows allowing the IR beam to pass through the wafer (16). The samples were activated in a stream of 25 ml/min He at 773 K for 30 min. A temperature ramp of 10 K/min was used. Pt-containing samples were—although pre-reduced as described above—reduced *in situ* in a stream of 20/80 H_2/He. Subsequently, the samples were cooled to 473 K. At this temperature pyridine was adsorbed by passing a stream of 25 ml/min He, containing 14 mbar of pyridine, over the catalyst. The high adsorption temperature was chosen in order to accelerate the diffusion of pyridine. After equilibrium was reached (5–30 min), weakly bound pyridine was desorbed for 1 h in 25 ml/min He. The uptake of pyridine was followed *in situ* by IR spectroscopy. Spectra were measured in the transmission/absorption mode, using a Nicolet SXB20 spectrometer (resolution 4 cm^{-1}). The relative concentration of Lewis and Brønsted acid sites was evaluated from the intensity of the bands at 1540 cm^{-1}, attributed to coordinatively bound pyridine, and at 1455 cm^{-1}, attributed to pyridinium ions (17), after desorption, using the absorption coefficients given by Khabtou *et al.* (18). The absolute concentration of acid sites was calculated by using a reference material (ZSM5, $SiO_2/Al_2O_3 = 80$) for which the concentration of acid sites (Brønsted + Lewis) had been determined by TGA (1).

In addition to the pyridine sorption experiments, the amount of tetrahedral and octahedral alumina was determined by solid-state ^{27}Al NMR. The experiments were performed on a Chemagnetics Infinity CMX-600 spectrometer operating at 156.33 MHz ($B_0 = 14.2$ T). The spectra were obtained using a 2.5-mm or a 3.2-mm Chemagnetics MAS probe, spinning at 25 kHz. Short-pulse excitations ($0.7\ \mu s = 0.056\pi$, $\nu_{rf} \sim 40$ kHz) were used to ensure quantitative excitation of the ^{27}Al resonances (19, 20) with 0.6- or 1.0-s relaxation delays and 100-kHz spectral width. Per measurement 3500–6000 free induction decays were collected. The ^{27}Al chemical shifts were determined relative to a standard of 1 M aqueous $Al(NO_3)_3$ solution.

Catalyst Testing

The parent MCM22 materials were first tested for their selectivity and activity in butene isomerization. For this purpose 10 mg of sample was mixed with about 60 mg quartz and put into a quartz reactor of 4 mm inner diameter. The sample was activated *in situ* in a flow of 25 ml/min at 830 K for 1 h and then cooled to 775 K. Then, the inlet stream was switched to a mixture of 7% 1-butene in Ar. The butene isomerization over MCM22 was followed for 3 h by GC analysis.

For dehydroisomerization experiments the sample was activated *in situ* in a flow of 25 ml/min H_2/Ar (20/80) at 830 K for 1 h and then cooled to reaction temperature. The reaction was carried out under the same conditions as in Ref. (5), i.e., 775 K and atmospheric pressure (unless otherwise noted). While higher temperatures would be more favorable for dehydrogenation (1), 775 K was chosen to avoid problems with the structural stability of MCM22 at higher temperatures (the calcination temperature was 813 K). The reaction mixture contained 10% *n*-butane, 20% hydrogen, the balance being Ar.

The reactor effluent was analyzed by gas chromatography, using an Al_2O_3 PLOT column for separation of the hydrocarbons in parallel with a Hayesep C and an MS5 Å column in series for the separation of hydrogen and other light gases. In the first minutes on stream the reactor effluent was stored in sample loops for postrun GC analysis. After 10 to 30 min, the reactor effluent was analyzed by direct injection into the GC at intervals of 45 min, without making use of the storage loops.

RESULTS

Catalyst Characterization

The Pt content and the SiO_2/Al_2O_3 ratio were determined by XRF (see Table 1). Traces of Fe (<0.03 wt%), Zr (<0.02 wt%), and Ti (<0.01 wt%) were found in all the samples. ν(OH), the intensity of the IR band at 3610 cm^{-1}, and the concentration of Brønsted acid sites determined by pyridine sorption (B) were proportional to each other

TABLE 1

Characterization of the (Pt–)MCM22 Materials

Sample	% Pt[a]	SiO_2/Al_2O_3[a]	Al (mmol/g)	ν(OH)[b] (a.u.)	B[b] (mmol/g)	L/(L + B)[b] (%)	$Al_{oh}/(Al_{oh} + Al_{td})$[c] (%)	Rel. crystallinity (%)[d] (102)	(302)
ST	**0.00**	**37.7**	**0.85**	**2.4**	**0.9**	**15**	**25**	**100**	**100**
	0.55	35.0	0.90	2.1	1.0	18	31	95	95
SR	**0.00**	**25.1**	**1.24**	**3.0**	**1.2**	**17**	**15**	**95**	**100**
	0.54	25.5	1.29	2.2 ± 0.3	1.1	22	26	65	65
	1.10	23.8	1.30	2.3 ± 0.2	1.1	22	29	75	70

Determined from [a] XRF, [b] IR, [c] ^{27}Al NMR, [d] XRD.

and decreased with the SiO_2/Al_2O_3 ratio of the samples. For both parent MCM22 materials approximately 15% of the total acid sites were Lewis acidic. The fraction increased slightly for the Pt-containing samples.

Figure 1 compares the powder XRD patterns of the parent MCM22s and 0.5% Pt–MCM22 SR. The assignment of the XRD reflections was taken from Ref. (21). The crystallinity of the two parent MCM22 materials did not differ significantly (see Table 1). MCM22 ST, however, had a higher fraction of octahedral Al (see Fig. 2), related to the presence of extraframework aluminum (22). Incorporation of Pt, i.e., ion-exchange, followed by calcination and reduction, did not significantly change the properties of MCM22 ST. In the case of MCM22 SR, however, dealumination occurred during the calcination/reduction procedure, as indicated by the increase in concentration of octahedral Al. The dealumination also led to a significant decrease in the crystallinity of the sample. A detailed comparison of the XRD patterns of the parent MCM22 and Pt–MCM22 showed that in Pt–MCM22 the intensities of lower indexed reflections (like (100)/(002) and (101)) decreased compared to those of the higher indexed reflections. This could point to a local destruction of the framework, which affected short-range reflections in XRD, while on a larger scale the structure was only slightly perturbed.

The relative concentration of Lewis acid sites measured by pyridine adsorption did not exactly agree with the ratio $Al_{oh}/(Al_{oh} + Al_{td})$. Especially in the case of MCM22 ST the concentration of octahedral Al was higher, indicating that not all the extraframework Al contributed to Lewis acidity.

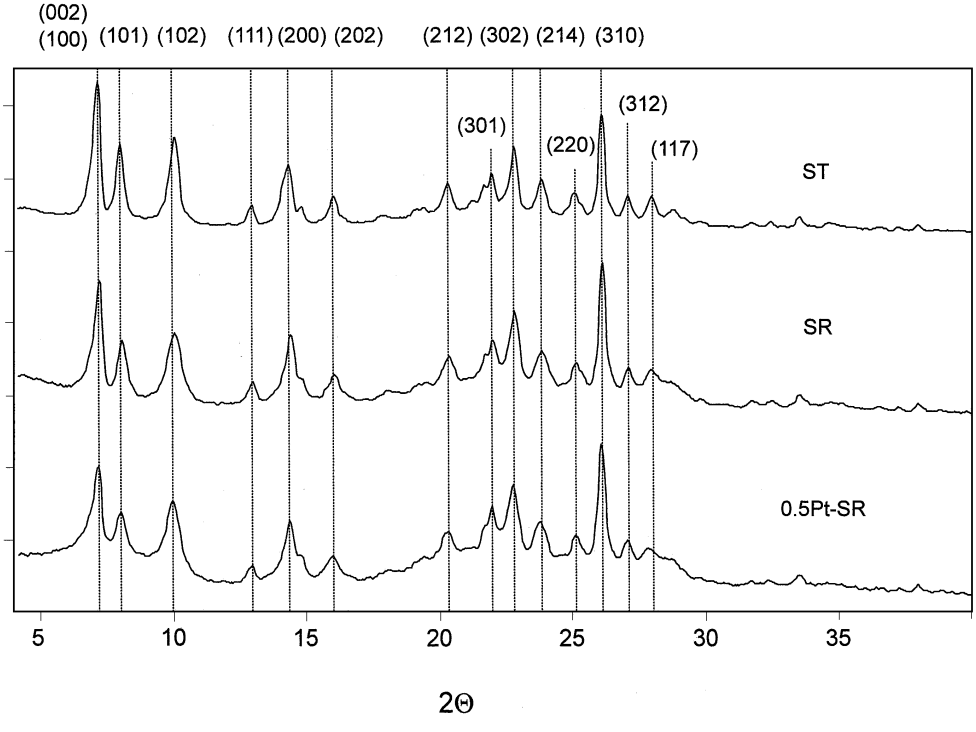

FIG. 1. XRD patterns of (a) MCM22 ST, (b) MCM22 SR, and (c) 0.5% Pt–MCM22 SR.

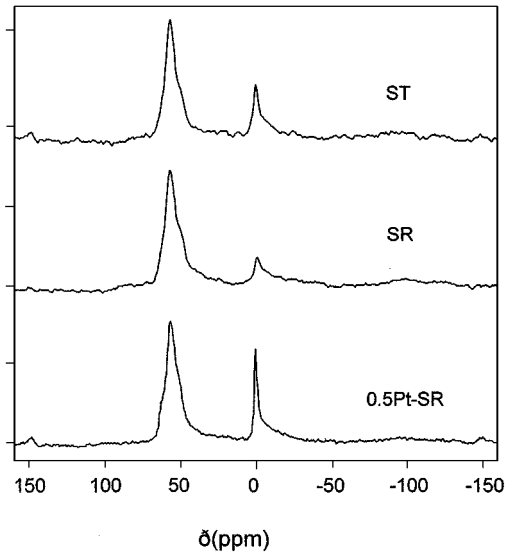

FIG. 2. ^{27}Al MAS NMR spectra of (a) MCM22 ST, (b) MCM22 SR, and (c) 0.5% Pt–MCM22 SR.

Butene Isomerization and Butadiene Poisoning

Figure 3 compares the performance of the MCM22 materials in the isomerization of 1-butene. For both catalysts the yield of isobutene increased drastically within the first minutes on stream. Simultaneously, the formation of by-products (mainly propene and pentene, and in the case of MCM22 SR also *n*-butane) decreased. After this period, stable yields of isobutene were obtained with MCM22 SR and ST, at excellent selectivity. Table 2 compares the activity and selectivity of the MCM22 materials with those of other isomerization catalysts (ZSM5, TON, FER) (5). The MCM22 catalysts were an order of magnitude more active and achieved higher yields of isobutene than the other materials at a comparable selectivity.

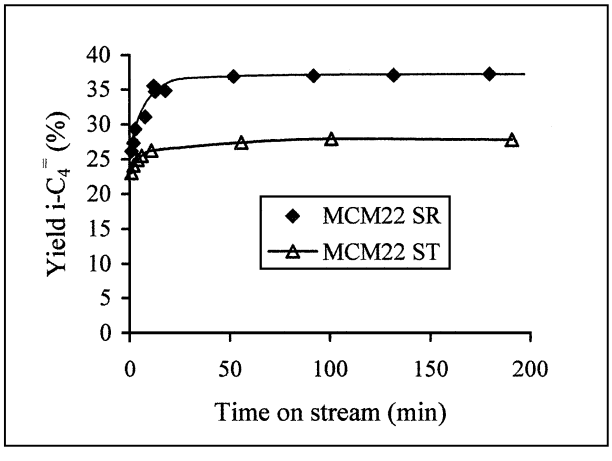

FIG. 3. Isomerization of 1-butene over MCM22. Conditions: 775 K, 1.2 bar, WHSV = 110 h^{-1}, ST = 2250 s g/m^3. Feed: 7% 1-butene in Ar.

TABLE 2

Comparison of Activity and Selectivity of Different Zeolites in Butene Isomerization

Sample	ST (s g/m^3)	Yield i-$C_4^=$ (%)	k[a] (m^3/s g)	Selectivity i-C_4^{2-} (%)
ZSM5(480)	5200	13.1	3.3×10^{-5}	87.1
TON(35)	4500	16.2	4.9×10^{-5}	88.6
FER(90)	4850	7.3	1.4×10^{-5}	94.3
FER(17)[b]	2400	14.8	9.2×10^{-5}	93.1
MCM22 (25) SR[c]	2500	37.0	$>1 \times 10^{-3}$	88.0
MCM22 (38) ST[c]	2250	28.0	$>6 \times 10^{-4}$	92.4

Conditions: SiO_2/Al_2O_3 ratio of the zeolites is given in parentheses, 775 K, 1 bar, 100 min on stream. Feed: 7% 1-butene in Ar.

[a] Pseudo-first-order rate constant of butene isomerization.

[b] 4.5% 1-butene in the feed instead of 7%.

[c] No data were measured at low conversions. As a result, only a lower limit of the rate constant could be given.

Dehydroisomerization of n-Butane

All four Pt–MCM22 materials listed in Table 1 were tested in the dehydroisomerization of *n*-butane under varying reaction conditions. Figure 4 shows a typical time-on-stream-behavior of 0.5% Pt–MCM22 ST. Initially, large amounts of methane and propane were formed. The rate of formation of these products decreased very fast. Simultaneously, the yield of the sum of butenes and of isobutene increased. After 20 min the performance of the catalyst was rather stable. The main products were linear butenes, isobutene, and isobutane.

From earlier investigations Pt–ZSM5 (0.5% Pt, $SiO_2/Al_2O_3 = 480$) had been found to be a good catalyst for the dehydroisomerization of *n*-butane (1). Figure 5 compares the steady-state performance (i.e., after 100 min on stream) of 0.5% Pt–MCM22 and 0.5% Pt–ZSM5(480). The dehydrogenation activities of the two Pt–MCM22 materials (ST and SR) and of Pt–ZSM5 were quite similar. The ratio i-$C_4^=/\sum C_4^=$, however, was much higher in the case of the Pt–MCM22s (see Fig. 5c). It came close to the thermodynamic limit at space times above 10,000 s g/m^3. As a result of the higher isomerization activity, higher yields of isobutene were obtained with Pt–MCM22 than with Pt–ZSM5 at the same contact time.

The by-product patterns of Pt–ZSM5 and Pt–MCM22 were quite different (see Fig. 6). For Pt–MCM22 isobutane was the most abundant by-product, as opposed to propane in the case of Pt–ZSM5. The total selectivity to by-products (i.e., all products apart from butenes) was comparable for the two materials.

The high selectivity to isobutane at low conversions suggests that it is a primary product formed by direct isomerization of *n*-butane on the acid sites. In order to check this, the reaction of *n*-butane over the parent MCM22 ST was performed under the same conditions as used in dehydroisomerization. Table 3 compares the yield of cracking products

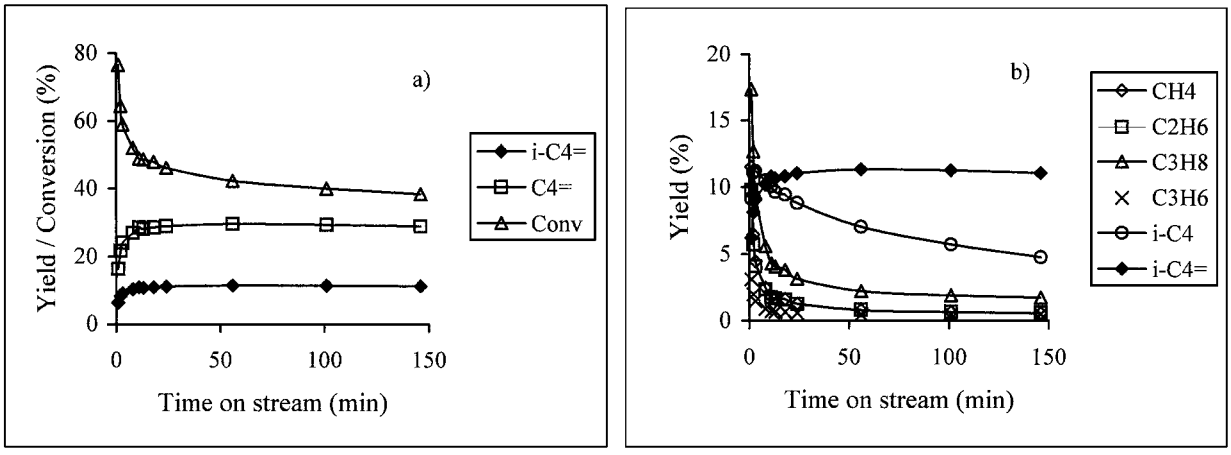

FIG. 4. Dehydroisomerization of *n*-butane over 0.5% Pt–MCM22 ST. Conditions: 775 K, 1 bar, WHSV = 23 h^{-1}. Feed: 10% *n*-butane, 20% H_2.

and the conversion of *n*-butane. The yield of isobutane was a factor of 40 smaller than in the presence of Pt. The yields of methane and ethane, cracking products of *n*-butane ($n\text{-}C_4H_{10} \rightarrow CH_4 + C_3H_6$, $C_4H_{10} \rightarrow C_2H_6 + C_2H_4$), were a factor of 10 lower. It was, therefore, concluded that (i) isobutane was not formed by isomerization of *n*-butane on the acid sites, but by hydrogenation of isobutene on Pt, and (ii) the contribution of protolytic cracking of *n*-butane on the acid sites to the overall by-product formation in dehydroisomerization was negligible.

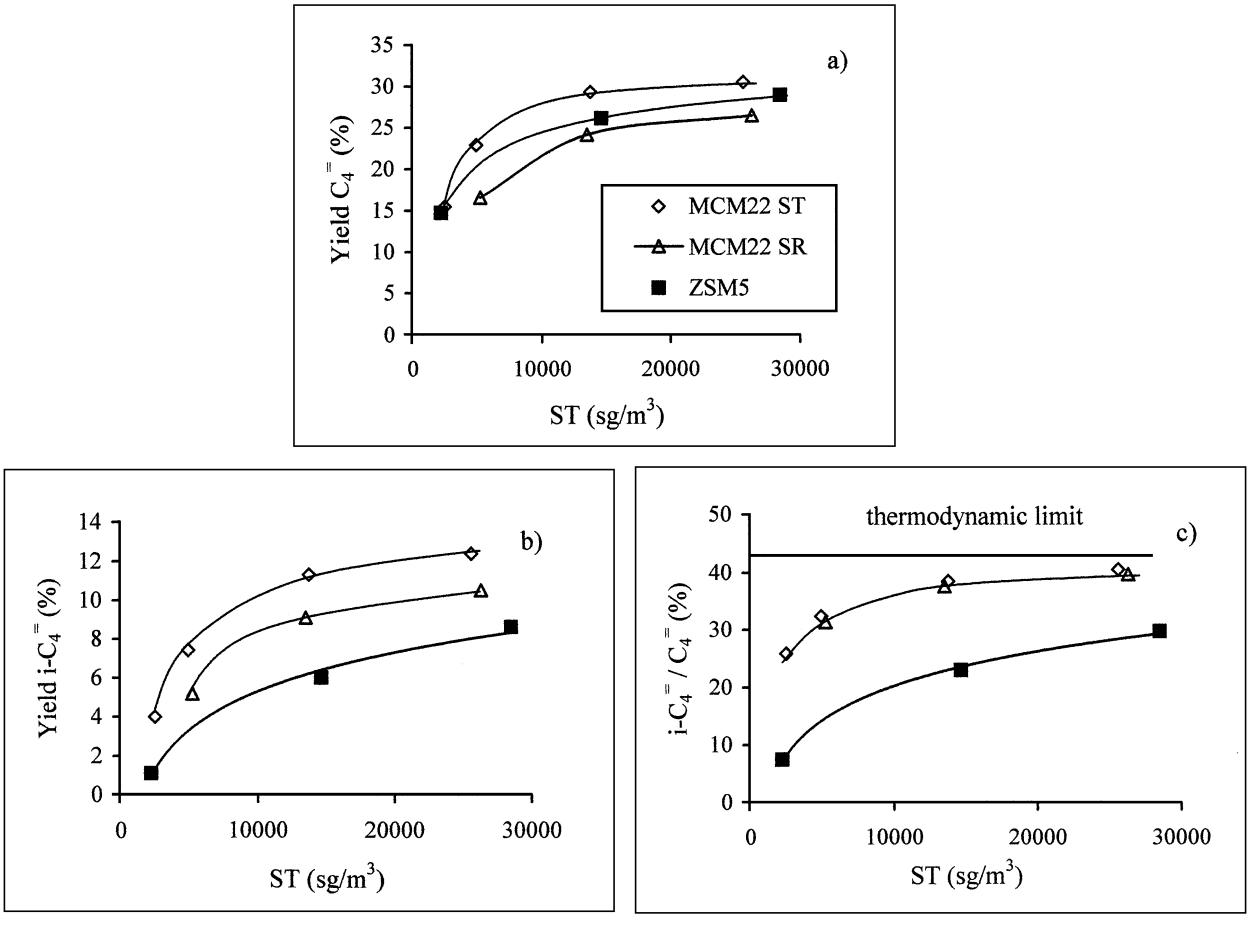

FIG. 5. (a) Yield of the sum of butenes, (b) yield of isobutene, and (c) ratio i-$C_4^=/\sum C_4^=$ as a function of the space time. Conditions: 775 K, 1 bar, 100 min on stream. Feed: 10% *n*-butane, 20% H_2. Metal loading of all three catalysts was 0.5% Pt.

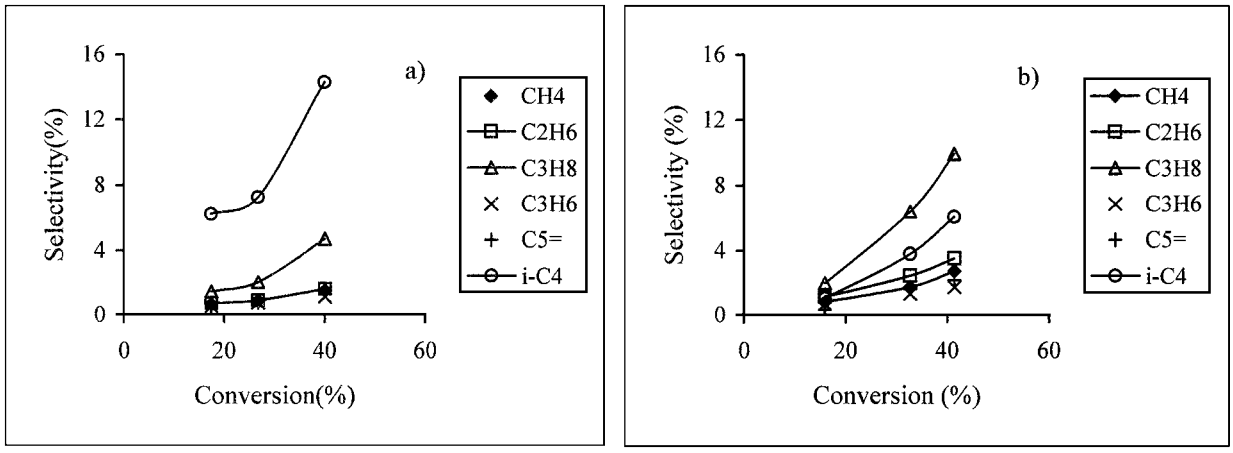

FIG. 6. Selectivity to by-products as a function of the conversion of *n*-butane. (a) 0.5% Pt–MCM22 ST and (b) 0.5% Pt–ZSM5(480). Conditions: 775 K, 1 bar, 100 min on stream.

Figure 7 compares the stabilities of Pt–MCM22 and Pt–ZSM5 during dehydroisomerization under identical reaction conditions. While the dehydrogenation activity of Pt–ZSM5 was stable, deactivation was observed for both Pt–MCM22 materials. It was much stronger for Pt–MCM22 SR than for ST. Increasing the metal loading of to 1% did not improve the stability of Pt–MCM22 SR.

Under the conditions shown in Fig. 7, the ratio i-$C_4^=$/ $\sum C_4^=$ was stable for all three catalysts. At higher WHSVs, however, a decrease in the isomerization activity of Pt–MCM22 was observed with time on stream. The rate of deactivation was higher with Pt–MCM22 SR than with Pt–MCM22 ST.

Dehydroisomerization over Pt–MCM22 ST was also performed at 825 K, where dehydrogenation is thermodynamically more favored than at 775 K (23). Under these conditions Pt–MCM22 ST achieved an initial yield of more than 16% isobutene. However, the dehydrogenation activity decayed much faster than at 775 K (see Fig. 8), in contrast to Pt–ZSM5.

TABLE 3

Yield of By-products in the Conversion of *n*-Butane over (Pt–)MCM22 ST

Yield (%)	MCM22 ST	Pt–MCM22 ST
CH_4	0.009	0.12
C_2H_6	0.014	0.13
C_2H_4	0.014	0.01
C_3H_8	0.000	0.26
C_3H_6	0.025	0.09
i-C_4	0.027	1.08
$\sum C_4^=$	0.041	15.5
Conversion (%)	0.13	17.4

Conditions: 775 K, 1.2 bar, WHSV = 180 h^{-1}, 100 min on stream. Feed: 10% *n*-butane, 20% H_2.

Dehydroisomerization over a Staged Bed of Pt–ZSM5 and MCM22

Previous studies (1) have shown high stability of Pt–ZSM5 in dehydroisomerization, but only a moderate selectivity. The results presented so far suggest an opposite behavior for Pt–MCM22. MCM22 was a very active and selective catalyst in butene isomerization, but the stability of Pt–MCM22 in dehydroisomerization was at best moderate, especially at higher temperatures (see Fig. 8). In trying to combine the stability of Pt–ZSM5 with the high isomerization activity of MCM22, staged bed experiments were performed, with a layer of Pt–ZSM5 upstream of a layer of MCM22 SR (the most active isomerization catalyst). A reaction temperature of 805 K was chosen in order to stay below the calcination temperature of MCM22 (813 K). Figure 9 compares the results of two-component catalysts with those of Pt–ZSM5 and Pt–MCM22.

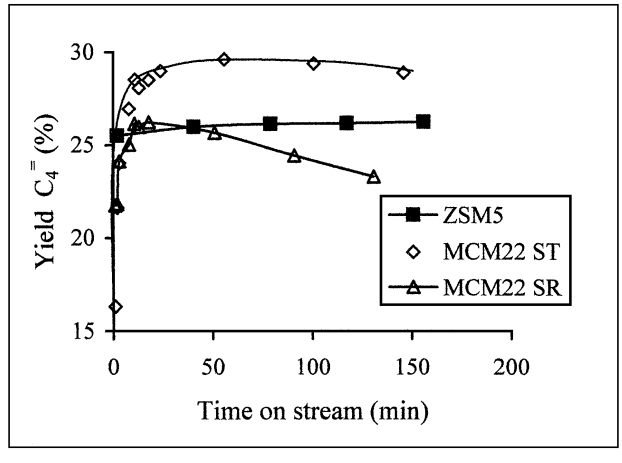

FIG. 7. Stability of dehydrogenation for Pt–MCM22 ST, Pt–MCM22 SR, and Pt–ZSM5(480). Metal loading was 0.5% for all three catalysts. Conditions: 775 K, 1 bar, WHSV = 25 h^{-1}. Feed: 10% *n*-butane, 20% H_2.

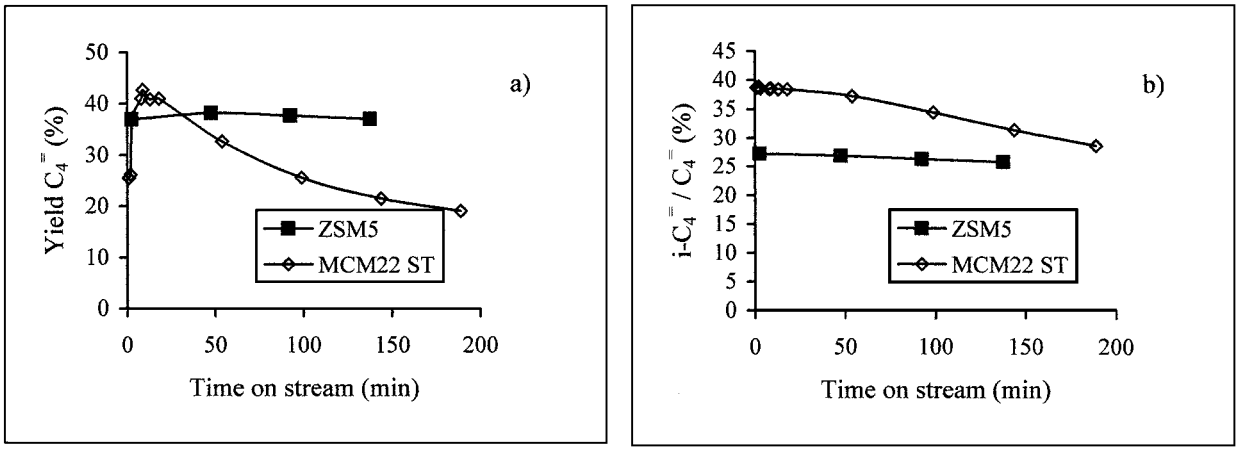

FIG. 8. Stability of (a) dehydrogenation and (b) isomerization for 0.5% Pt–MCM22 ST and 0.5% Pt–ZSM5(480). Conditions: 825 K, 1 bar, WHSV = 20 h^{-1}. Feed: 10% *n*-butane, 20% H_2.

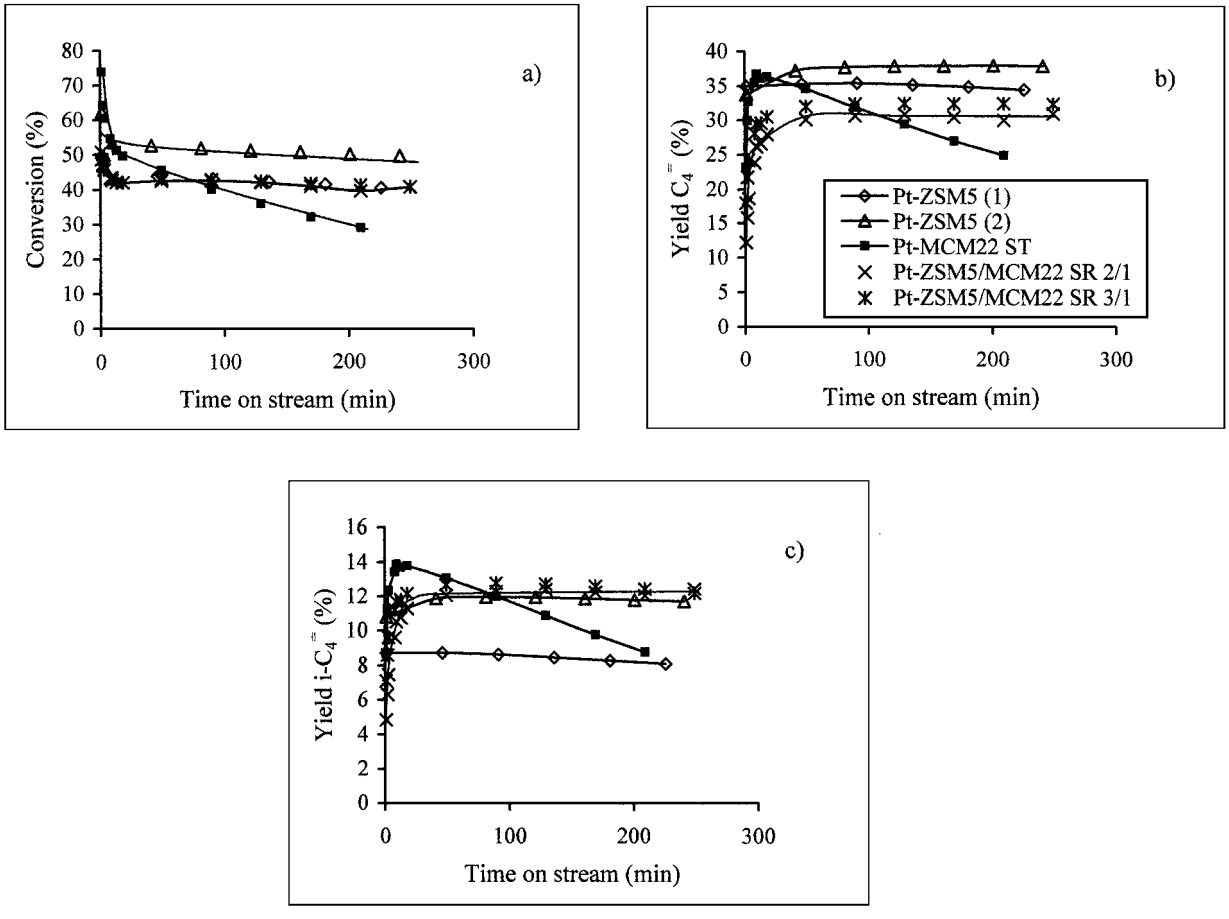

FIG. 9. Dehydroisomerization of *n*-butane over Pt–MCM22 ST, Pt–ZSM5, and a staged bed Pt–ZSM5/MCM22 SR ($m/m = 3/1$ and 2/1). Metal loading of all catalysts was 0.5% Pt. (a) Conversion of *n*-butane. (b) Yield of $\sum C_C^=$. (c) Yield of isobutene. Conditions: 805 K, 1.0 bar, WHSV = 25 h^{-1} (12.5 h^{-1} for Pt–ZSM5(2)). Feed: 10% *n*-butane, 20% H_2.

TABLE 4

Dehydroisomerization of *n*-Butane over Pt–MCM22 ST, Pt–ZSM5, and a Staged Bed of Pt–ZSM5/MCM22 SR

	Pt–MCM22 ST	Pt–ZSM5		Pt–ZSM5/MCM22 3/1	Pt–ZSM5/MCM22 2/1
WHSV (h^{-1})	25	25	12.5	25	25
Yield $\sum C_4^=$ (%)	25.0	34.6	38.0	32.4	30.5
Yield i-$C_4^=$ (%)	9.0	8.1	11.8	12.4	12.0
i-$C_4^=/\sum C_4^=$	35.5	23.5	31.0	38.5	40.1
Sel. $\sum C_4^=$ (%)	86	84	76	78	76
Sel. i-$C_4^=$	30	23.5	20	30	30

Conditions: 805 K, 1.0 bar, 200 min on stream. Feed: 10% *n*-butane, 20% H_2, balance Ar.

Due to the low activity of MCM22 in cracking of *n*-butane the additional bed of MCM22 SR did not lead to a higher *n*-butane conversion compared to Pt–ZSM5. Only the butenes formed on Pt–ZSM5 underwent secondary transformation over MCM22, i.e., cracking, mainly to ethene and propene, and isomerization. Because of the cracking reactions, the yield of $\sum C_4^=$ decreased slightly from Pt–ZSM5 to the 3/1 and 2/1 mixture with MCM22 SR. The yield of isobutene, on the other hand, increased significantly from 8 to 12.5% upon addition of MCM22 SR (see Table 4). Note that increasing the MCM22 content in the staged bed from 25 to 33 wt% did not lead to a further increase in the yield of isobutene, but only in the yield of cracking products.

A yield of 12.5% isobutene could also be obtained with Pt–ZSM5, when the contact time was doubled (see Table 4). But in that case the selectivity to isobutene was significantly lower than that with the staged bed (23.5% compared to 30% for the staged bed).

Pt–MCM22 ST gave initially the highest yield of isobutene (14%). But, as at 825 K, the dehydrogenation activity decayed very fast, while the staged bed was stable.

DISCUSSION

ZSM5 is only a moderately well suited catalyst for the isomerization of butenes. As butene isomerization approaches thermodynamic equilibrium, the selectivity of ZSM5 to oligomerization/cracking products (mainly propene and pentene) increases exponentially (24, 25). That is also the reason why, in dehydroisomerization of *n*-butane over Pt–ZSM5, oligomerization/cracking increases drastically as the ratio of i-$C_4^=/\sum C_4^=$ approaches thermodynamic equilibrium (1). This limits the yield of isobutene that can be achieved.

MCM22, on the other hand, reached i-$C_4^=/\sum C_4^=$ ratios of up to 39% in the skeletal isomerization of 1-butene, close to the thermodynamic limit of 43%, while maintaining a high selectivity of around 90%. At similar ratios of i-$C_4^=/\sum C_4^=$ the selectivity of ZSM5 was only 60%. It is therefore to be expected that a Pt–MCM22 catalyst used for the dehydroisomerization of *n*-butane should suffer much less from loss in selectivity by oligomerization/cracking reactions of butenes. This was fully confirmed by the reported findings. While Pt–MCM22 and Pt–ZSM5 gave comparable yields of $\sum C_4^=$, the yield of isobutene was higher for Pt–MCM22, due to the higher isomerization activity of MCM22. Very few cracking products were observed even at high conversions. The main by-product of Pt–MCM22 was isobutane, formed by hydrogenation of isobutene on the metal, as opposed to propane in the case of Pt–ZSM5, which is formed by oligomerization/cracking and subsequent hydrogenation. In explaining the catalytic properties of (Pt–)MCM22 two questions have to be addressed. (i) Why is the intrinsic selectivity of MCM22 to isomerization vs oligomerization/cracking higher than that for ZSM5? (ii) What are the reasons for the different behavior of Pt–MCM22 as compared to that of Pt–FER, which is also a very selective catalyst for butene isomerization?

Let us first turn to the high activity and selectivity of MCM22 in butene isomerization. In the case of ZSM5 it is usually argued that the moderate selectivity of this material in butene isomerization is related to the cavities (inner diameter 6–7 Å) formed at the intersections of straight and sinusoidal channels, which are sufficiently large to allow formation of larger molecules, which subsequently crack unselectively. In the light of this argument, the high selectivity of MCM22 is surprising, since the interlayer pore system of MCM22 contains even larger cavities (diameter 18 Å). MCM22 was, however, only selective in steady-state (see Fig. 3). Initially, the by-product formation was very high. It is, thus, possible that the interlayer channel system with the large cages was rapidly deactivated in the initial stages of the reactions. Subsequently, the reaction took place only in the intralayer channel system. The dimensions of this channel system (5.5×4.0 Å) are smaller than those in the case of ZSM5 (5.3×5.6 Å and 5.1×5.5 Å) and comparable to those of FER (4.2×5.4 Å), explaining the high selectivity to butene isomerization. Moreover, the pore system of MCM22 is two-dimensional, which facilitates diffusion of the molecules, and could be responsible for higher activity of MCM22 compared to FER and TON (see Table 2).

The question of higher dehydrogenation activity of Pt–ZSM5 and Pt–MCM22 compared to Pt–FER seems to be related to diffusion. In the case of Pt–FER most of the Pt was present in the form of small particles in the zeolite pores. Due to the large zeolite crystals (6–10 μm) diffusion pathways were long. As a result, access to the metal was constrained (5). SEM photographs of MCM22 showed that the dimensions of the layers were rather small (0.5–1 μm). Moreover, the two-dimensionality of the pore system facilitates diffusion. Regarding the distribution of Pt

over the material, high-resolution electron microscopy images of the Pt–MCM22 samples indicated a bimodal particle size contribution, with larger Pt clusters on the external surface and small metal particles inside the zeolite pores, similar to the distribution found for Pt–ZSM5 (5). Due to the two-dimensionality of the pore system, the short diffusion pathways, and the distribution of metal inside and outside the pores, access to the metal was not constrained and a high dehydrogenation activity was obtained, like in the case of Pt–ZSM5.

Apart from activity and selectivity, also the stability is a very important issue for the practical use of a catalyst. In this respect the performance of Pt–MCM22 was only moderate, especially at higher temperatures. The dehydrogenation and isomerization activity decreased faster for Pt–MCM22 SR than for Pt–MCM22 ST. In the skeletal isomerization of butene, in contrast, MCM22 ST and SR showed stable performance. The observed deactivation in the dehydroisomerization reaction was, thus, attributed to structural changes caused during calcination/reduction of Pt–MCM22. Note that the concentration of octahedral Al in MCM22 SR increased significantly upon incorporation of Pt (see Table 1), indicating that the framework was dealuminated. XRD showed a concomitant loss in crystallinity. The framework structure of MCM22 ST was apparently less affected during the calcination/reduction of Pt and maintained a rather stable isomerization and dehydrogenation activity, in contrast to Pt–MCM22 SR. This suggests that the deactivation is strongly related to the crystallinity of the samples. Enhanced deactivation of dealuminated samples was also observed in the skeletal isomerization of *n*-butene over ferrierites modified by steaming (26) and for dealuminated TON (27).

We can only speculate about the mechanism of deactivation of Pt–MCM22. In the dehydroisomerization experiments a higher formation of aromatics (benzene and toluene) was observed for Pt–MCM22 than for Pt–ZSM5. The formation of benzene and toluene rapidly decreased with time on stream. The selectivity to aromatics and the rate of deactivation of the metal both increased with increasing temperature. It is therefore possible that aromatics initially formed on Pt were slowly transformed to coke, thereby deactivating the metal sites. The decrease in isomerization activity could be explained by a blocking of the zeolite pores by the coke species. Remember that the pores of MCM22 are smaller than those of ZSM5 and can be blocked more easily by aromatic species.

In order to circumvent the problems with deactivation of Pt–MCM22 at high temperatures, the use of MCM22 as an additional isomerization catalyst in combination with Pt–ZSM5 is a very interesting alternative. In such a staged bed Pt–ZSM5 should mainly act as a dehydrogenation catalyst, while the ratio $i\text{-}C_4^= / \sum C_4^=$ has to be kept low in order to avoid extensive by-product formation. The MCM22 content should be chosen high enough to bring the ratio $i\text{-}C_4^= / \sum C_4^=$ close to thermodynamic equilibrium. A too high MCM22 content, however, will lead to unnecessary cracking reactions of butene and will lower the selectivity. Pt–ZSM5 can achieve yields of isobutene similar to those obtained with the staged bed, but only at significantly higher contact times and, hence, with a lower selectivity to isobutene.

CONCLUSIONS

MCM22 is a very active and selective catalyst for butene isomerization at high temperatures. Its high selectivity and activity are attributed to the shape-selective properties of the 10-membered-ring channels in the layers, whose dimensions are similar to those of FER, and to the two-dimensionality of the pore system of MCM22 which facilitates diffusion.

The good catalytic properties of MCM22 in butene isomerization can be successfully made use of in the dehydroisomerization of *n*-butane over Pt–MCM22. Due to the higher activity and selectivity of MCM22 in butene isomerization compared to those of ZSM5, Pt–MCM22 gives higher yields of isobutene than Pt–ZSM5 and fewer oligomerization/cracking products. The contribution of the other possible side reaction, protolytic cracking of *n*-butane on the acid sites and hydrogenolysis on the metal, is negligible.

The deactivation of the dehydrogenation and isomerization activity of Pt–MCM22 during dehydroisomerization is attributed to defects created in the material. The good catalytic properties of MCM22 can be maintained only when the framework remains intact during calcination/reduction of Pt–MCM22. The observed differences between Pt–MCM22 SR and ST were mainly related to the different deactivation behavior, i.e., the different crystallinity, of these samples. The SiO_2/Al_2O_3 ratio, on the other hand, had only a minor influence of the performance, at least within the reported range of variation (24 to 35).

As an alternative to a bifunctional Pt–MCM22, the parent MCM22 can also be used as a pure isomerization catalyst in combination with Pt–ZSM5 in order to increase the yield of isobutene in dehydroisomerization, in analogy to the staged bed approach of Bellussi *et al.* (28). The two-component catalyst has a significant advantage over Pt–ZSM5 with respect to selectivity and activity in isobutene formation and does not suffer from deactivation, like Pt–MCM22.

ACKNOWLEDGMENTS

This work was performed under the auspices of NIOK, the Netherlands Institute of Catalysis Research. IOP Katalyse (IKA 94023) is gratefully acknowledged for financial support. The authors are very much indebted to Prof. Weitkamp, from the University of Stuttgart, and to

Dr. Nowak, from Shell Research and Technology Center Amsterdam, for supplying the MCM22 samples. NMR experiments were performed at the NOW/CW HF-NMR Facility (NSR Center, University of Nijmegen). Mrs. G. H. Nachtegaal is thanked for skillfully designing and performing the NMR experiments, and O. P. E. Zinck-Stagno for his help in preparing the Pt–MCM22 samples.

REFERENCES

1. Pirngruber, G. D., Seshan, K., and Lercher, J. A., *J. Catal.* **186**, 188 (1999).
2. Mooiweer, H. H., de Jong, K. P., Kraushaar-Czarnetzki, B., Stork, W. H. J., and Krutzen, B. C. H., *in* "Zeolites and Related Microporous Materials: State of the Art 1994" (J. Weitkamp, H. G. Karge, H. Pfeifer, and H. Hölderich, Eds.), Stud. Surf. Sci. Catal., Vol. 84, p. 2327. Elsevier, Amsterdam, 1994.
3. Grandvallet, P., de Jong, K. P., Mooiweer, H. H., Kortbeek, A. G. T., and Kraushaar-Czarnetzki, B., EP Patent 501.577 (1992), assigned to Shell Internationale Research Maatschappij B.V.
4. Barri, S. A. I., Walker, D. W., Tahir, R., EP Patent 247.802 (1990), assigned to The British Petroleum Co.
5. Pirngruber, G. D., Seshan, K., and Lercher, J. A., *J. Catal.* **190**, 374 (2000).
6. Leonowicz, M. E., Lawton, J. A., Lawton, S. A., and Rubin, M. K., *Science* **264**, 1910 (1994).
7. Martens, J. A., Tielen, M., Jacobs, P. A., and Weitkamp, J., *Zeolites* **4**, 98 (1984).
8. Martens, J. A., and Jacobs, P. A., *Zeolites* **6**, 334 (1986).
9. Souverijns, W., Verrelst, W., Vanbutsele, G., Martens, J. A., and Jacobs, P. A., *J. Chem. Soc., Chem. Commun.* 1671 (1994).
10. Thomas, J. M., *Sci. Am.* **April**, 112 (1992).
11. Houzvicka, J., Hansildaar, S., and Ponec, V., *J. Catal.* **167**, 273 (1997).
12. Asensi, M. A., Corma, A., and Martinez, A., *J. Catal.* **158**, 561 (1996).
13. Corma, A., Corell, C., and Perez-Pariente, J., *Zeolites* **15**, 2 (1995).
14. Hunger, M., Ernst, St., and Weitkamp, J., *Zeolites* **15**, 188 (1995).
15. Abril, R. P. L., Bowes, E., Green, G. J., Marler, D. O., Sihabi, D. S., and Sacha, R. F., US Patent 5.085.762 (1992), assigned to Mobil.
16. Mirth, G., Eder, F., and Lercher, J. A., *Appl. Spectrosc.* **48**, 194 (1994).
17. Ward, J. W., *J. Catal.* **9**, 225 (1967); **11**, 271 (1968).
18. Khabtou, S., Chevreau, T., and Lavalley, J. C., *Microporous Mater.* **3**, 133 (1994).
19. Samoson, A., and Lippmaa, E., *Chem. Phys. Lett.* **100**, 205 (1983).
20. Samoson, A., and Lippmaa, E., *Phys. Rev. B* **28**, 6567 (1983).
21. Lawton, St. L., Fung, A. S., Kennedy, G. J., Alemany, L. B., Chang, C. D., Hatzikos, G. H., Lissy, D. N., Rubin, M. K., Timken, H. K. C., Steuernagel, S., and Woessner, D. E., *J. Phys. Chem.* **100**, 3788 (1996).
22. Engelhardt, G., *in* "Introduction to Zeolite Science and Practice" (H. van Bekkum, E. M. Flanigen, and J. C. Jansen, Eds.), p. 285. Elsevier, Amsterdam, 1991.
23. Pirngruber, G. D., Seshan, K., and Lercher, J. A., *J. Catal.* **190**, 338 (2000).
24. Pirngruber, G. D., Seshan, K., and Lercher, J. A., *Catal. Lett.*, in press.
25. Houzvicka, J., Nienhuis, J. G., and Ponec, V., *Appl. Catal. A* **174**, 207 (1998).
26. Xu, W.-Q., Yin, Y.-G., Suib, St. L., Edwards, J. C., and O'Young, Ch.-L., *J. Catal.* **163**, 232 (1996).
27. Baeck, S. H., and Lee, W. Y., *Appl. Catal. A* **168**, 171 (1998).
28. Bellussi, G., Giusti, A., and Zanibelli, L., US Patent 5.336.803 (1994), assigned to Eniricerche SpA, Snamprogetti SpA.